

Article

Shape-Controlled Crystal Growth of $Y_3Al_5O_{12}:Ce$ Single Crystals with Application of Micro-Pulling-Down Method and Mo Crucibles, and Their Scintillation Properties

Masao Yoshino ^{1,2,*} , Atsushi Kotaki ³, Yuui Yokota ³ , Takahiko Horiai ^{1,2} and Akira Yoshikawa ^{1,2,3}¹ New Industry Creation Hatchery Center, Tohoku University, Sendai 980-0879, Japan² C&A Corporation, Sendai 980-0811, Japan³ Institute for Materials Research, Tohoku University, Sendai 980-8577, Japan

* Correspondence: yoshino.masao@tohoku.ac.jp; Tel.: +81-22-215-2214

Abstract: The technology to grow single crystals of the required shape directly from a melt has been researched extensively and developed in various industries and research fields. In this study, a micro-pulling-down method and a Mo crucible were applied to the shape-controlled crystal growth of $Y_3Al_5O_{12}:Ce$ (YAG:Ce). Three types of Mo crucibles with different die shapes were developed. Stable crystal growth of more than 50 mm in length was achieved with the same shape as the die, and scintillation light output of ~20,000 ph/MeV, which is comparable with those of the YAG:Ce crystal grown by Cz method, were obtained. The transmittance of grown crystals above 500 nm was above 70%. The standard deviation (σ) of the scintillation light output at each position of the 50-mm-long sample was found to be within $\pm 16\%$.

Keywords: micro-pulling-down method; shape-controlled crystal growth; scintillator materials; Mo crucibles



Citation: Yoshino, M.; Kotaki, A.; Yokota, Y.; Horiai, T.; Yoshikawa, A. Shape-Controlled Crystal Growth of $Y_3Al_5O_{12}:Ce$ Single Crystals with Application of Micro-Pulling-Down Method and Mo Crucibles, and Their Scintillation Properties. *Crystals* **2022**, *12*, 1215. <https://doi.org/10.3390/cryst12091215>

Academic Editor: Fapeng Yu

Received: 2 August 2022

Accepted: 23 August 2022

Published: 28 August 2022

Publisher's Note: MDPI stays neutral with regard to jurisdictional claims in published maps and institutional affiliations.



Copyright: © 2022 by the authors. Licensee MDPI, Basel, Switzerland. This article is an open access article distributed under the terms and conditions of the Creative Commons Attribution (CC BY) license (<https://creativecommons.org/licenses/by/4.0/>).

1. Introduction

Inorganic scintillators have been applied as radiation imaging sensors in many fields [1–3]. Some studies have developed imaging techniques that use scintillator arrays as collimators [4,5]. A tube-shaped single-crystal scintillator was required in these studies to achieve a high image quality. Scintillators that are used in medical applications are typically cut and polished from a large bulk single-crystal form and assembled into radiation detectors. The Czochralski [6,7], Bridgman–Stockbarger [8], and Floating Zone [9] methods are commonly used as crystal-growth techniques to obtain large bulk crystals. However, it is difficult to process large single-crystal scintillators into a tube, which has been an obstacle to the production of tube-shaped scintillators.

The technology to grow single crystals of the required shape directly from the melt has been researched extensively and developed in various industries and research fields. Edge-defined film-fed growth (EFG) [10,11] and micro-pulling-down (μ -PD) methods [12–16] are examples of such technology. The μ -PD method is a crystal growth technique that uses a crucible with a die with several holes in the bottom to supply the melt. The μ -PD provides the growth of long single crystals with a ready to use shape without any cutting and polishing. It is possible to control the crystal shape with the same cross-sectional shape as the die. In our recent research, we succeeded in growing a tubular $Y_3Al_5O_{12}:Ce$ (YAG:Ce) single-crystal scintillator, which can be used for novel medical imaging techniques, by the μ -PD method and Ir crucible [17]. O. Sidletskiy et al. reported the μ -PD growth of long $Y_3Al_5O_{12}$ - and $Lu_3Al_5O_{12}$ -based fibres [18]. On the other hand, the recent price of iridium metal used in the crucibles in the previous study has soared more than five times compared to five years ago. The price hike of iridium metal used for the crucible is a very serious problem for the mass production of single crystals. As an alternative to precious metals

such as Ir, crystal growth that uses inexpensive crucibles such as Mo is promising, and the growth of YAG:Ce single crystals using Mo crucibles has been reported recently [19].

In this study, the μ -PD method and Mo crucibles with different die shapes were applied to growing tube shaped-controlled YAG:Ce (tube-YAG:Ce) single-crystal scintillators. The optical and scintillation properties of the grown crystals were evaluated.

2. Materials and Methods

2.1. Mo Crucible with a Tube-Shaped Die

The design drawings of the developed Mo crucible are shown in Figure 1a. We developed three types of Mo crucibles with different die shapes (Figure 1b). The TYPE1 crucible has a round die shape, and the TYPE2 and TYPE3 crucibles have a square die shape. By using these crucibles, we investigated the effect of die shape on crystal growth.

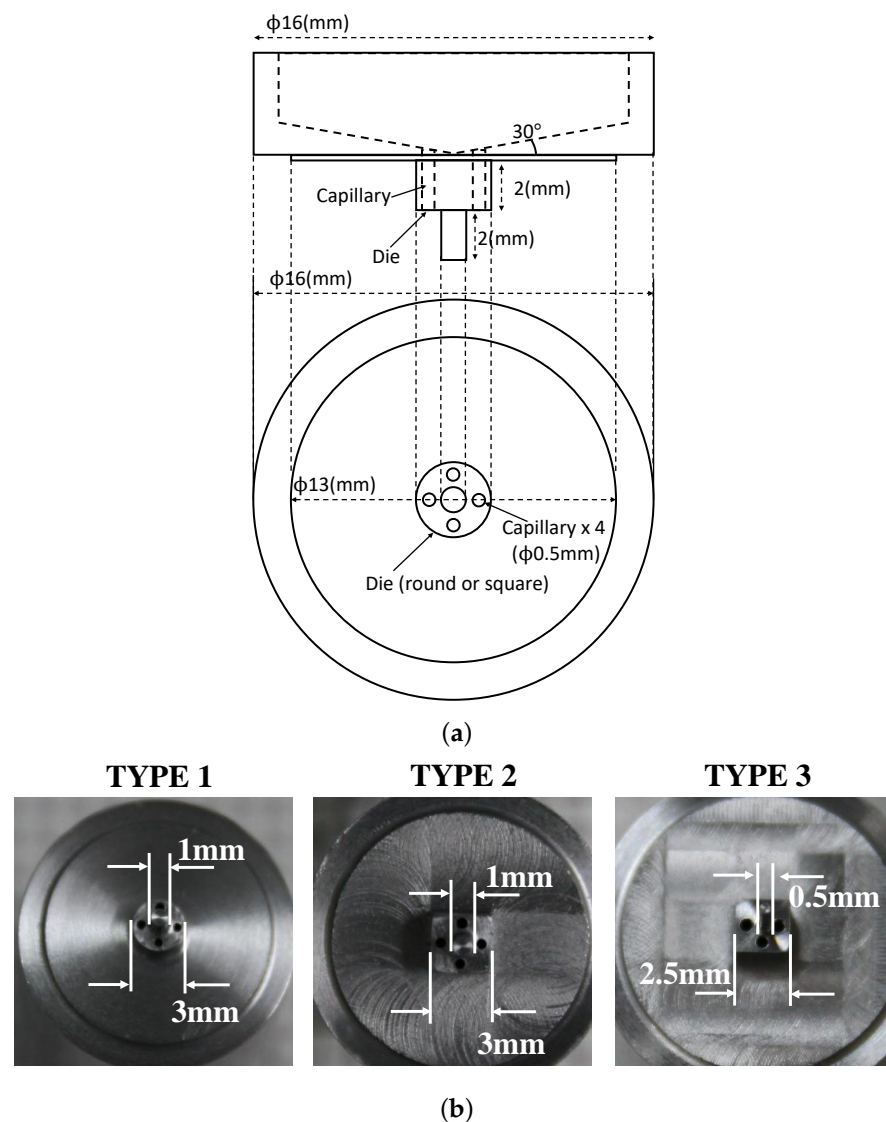


Figure 1. (a) Design drawing and (b) photographs of developed Mo crucibles.

2.2. Crystal Growth Setup

The μ -PD method was applied to grow tube-YAG:Ce single crystals. Powder starting materials α - Al_2O_3 , Y_2O_3 , and CeO_2 (purity 4N or higher) were weighed out and mixed to obtain nominal compositions of $(\text{Y}_{0.995}\text{Ce}_{0.005})_3\text{Al}_5\text{O}_{12}$. The mixed powder was placed in a crucible and heated to the melting point of YAG:Ce by using a high-frequency induction coil. An Ar + H_2 atmosphere was used to prevent the Mo crucibles from oxidizing during

crystal growth. The seed crystals were (0 0 1)-oriented YAG:Ce 1.0% single crystals. A schematic diagram of the μ -PD crystal growth assembly is provided in Figure 2. The growth rate varied from 0.1 mm/min to 0.5 mm/min to grow tube-shaped crystals. The grown tube-YAG:Ce single crystals were cut perpendicular to the growth direction and polished to produce evaluation samples for characterization.

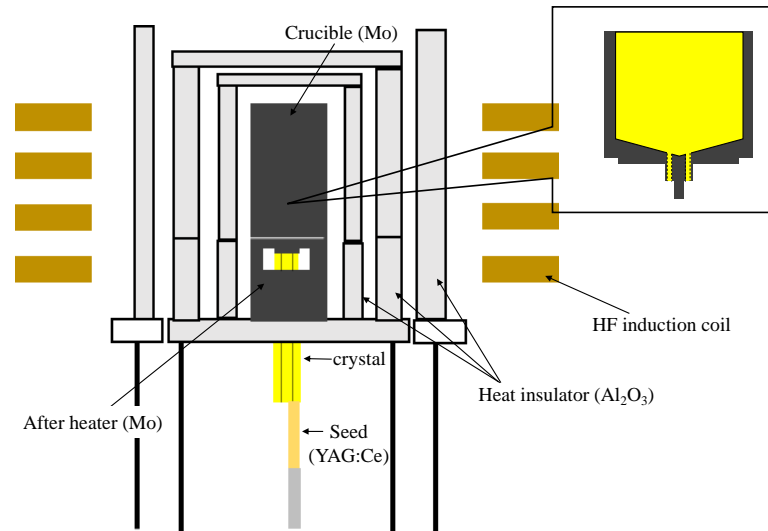


Figure 2. Schematic diagram of crystal-growth assembly.

2.3. Characterization

The chemical composition of the polished sample surface was analyzed by using a field emission electron probe microanalyzer (FE-EPMA, JXA-8530F, JEOL Ltd., Tokyo, Japan) to evaluate the radial Ce distribution. The detection limit of the FE-EPMA measurement was 210 wt. ppm. Transmittance spectra were measured from 200 to 750 nm by using a UV/VIS spectrophotometer (V-550, JASCO Corp., Tokyo, Japan). The thickness of the sample for transmittance measurement was set to 1.0 mm. Scintillation lights were collected by a photomultiplier tube (PMT, R7600-200, Hamamatsu Photonics K.K., Hamamatsu, Japan) with an operating voltage of 600 V. A 10 MBq ^{137}Cs source was used at a distance of 5 cm. The signal from the PMT was amplified by a spectroscopy amplifier (MSCF-16, mesytec GmbH & Co.KG, Wernher-von-Braun-Str. 1, D-85640 Putzbrunn, Germany), and digitized by a peak-digital-converter (PDC) (A3400, NIKI GLASS Co., Ltd., Tokyo, Japan). The scintillation waveforms were recorded by using a digital oscilloscope (RTB2004, Rohde & Schwarz GmbH & Co.KG, Munich, Germany). The decay time was calculated by fitting a sum of two exponential functions to the waveform:

$$A(t) = A_1 \exp(-t/\tau_1) + A_2 \exp(-t/\tau_2) + \text{const}$$

The values A_1 , A_2 and τ_1, τ_2 are the amplitudes and decay times of the waveforms, respectively.

3. Results

3.1. Crystal Growth

The crystal growth of the tube-YAG:Ce single crystals was achieved by the μ -PD method. After the starting material had been melted in a Mo crucible, the melt passed through capillaries to reach the die at the bottom of the crucible. The seed crystal was touched to the melt at the bottom of the die to form a meniscus between the bottom of the die and the seed crystal. The crystals were grown continuously by pulling down the seed crystal with a moderate temperature gradient near the liquid–solid interface (Figure 3). In the early stage of crystal growth (Figure 3a), the spreading of the meniscus to the

bottom of the crucible was unstable, which resulted in an inconsistent outer diameter of the grown crystals. Figure 3b shows the solid–liquid interface when the meniscus thickness was stabilized by optimizing the power of the high-frequency (HF) induction coil and the pulling-down rate. The meniscus height after stable growth was kept at 80–100 μm . Photographs of the grown crystals and samples that were cut perpendicular to the growth direction are shown in Figure 3c. The cross-sectional shape of the grown crystals was like the shape of the bottom of the die. A comparison of the crystal growth in the TYPE1 and TYPE2 crucible shows the effect of die shape on crystal growth as a function of pulling-down speed for stable crystal growth. The pulling-down speed to stabilize crystal growth was faster in the crucible with a square die (0.5 mm/min) than in the crucible with a round die (0.1 mm/min). Growth using the TYPE3 crucible was conducted at 0.2 mm/min and 0.5 mm/min. At a slow growth rate (0.2 mm/min), the meniscus was wetted and spread at the tip of the protrusion, and the inside of the tube crystal was filled with melt. At high growth rates (0.5 mm/min), the inside of the tube crystal was not filled with melt because the wetting spread of the meniscus to the tip of the protrusion was suppressed (Figure 4). By using TYPE3 crucible and optimizing the crystal growth rate, stable crystal growth of more than 50 mm in length was achieved with the same shape as the die.

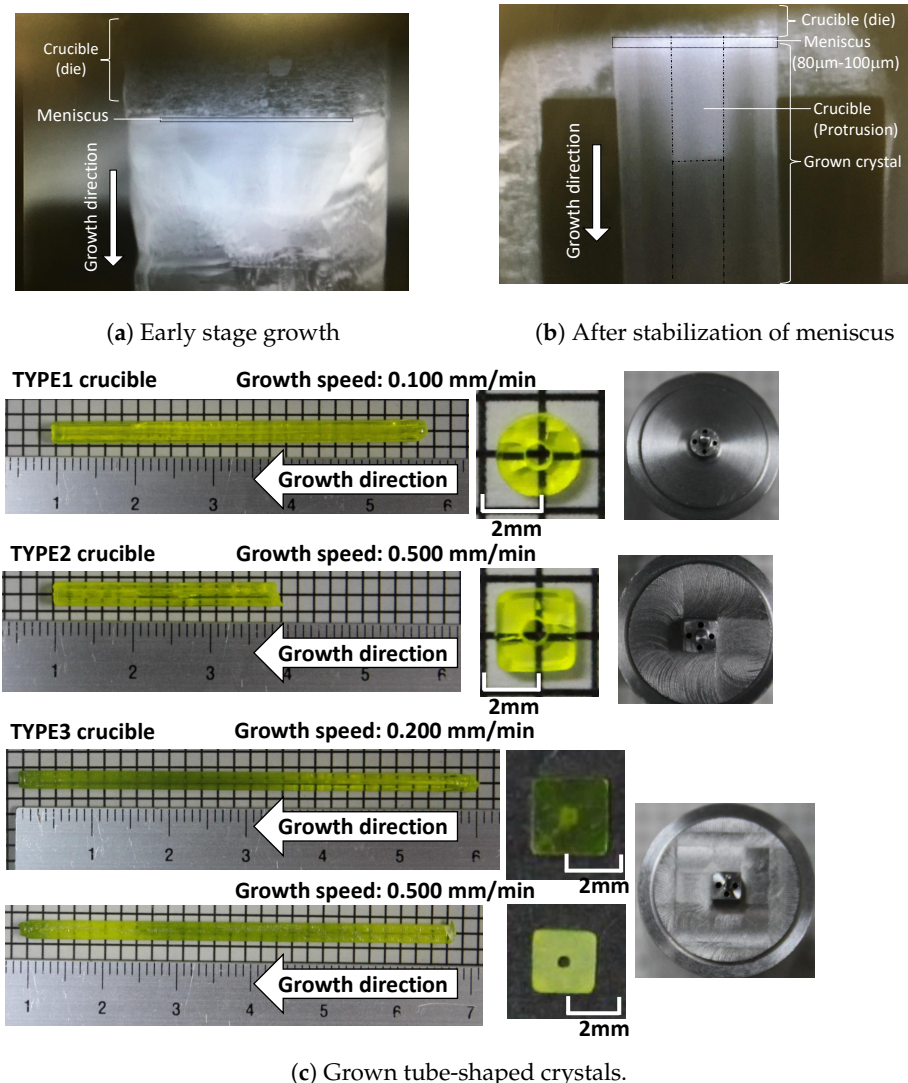


Figure 3. (a,b) Liquid–solid interface during crystal growth and (c) tube-shaped crystals grown by three types of Mo crucibles.

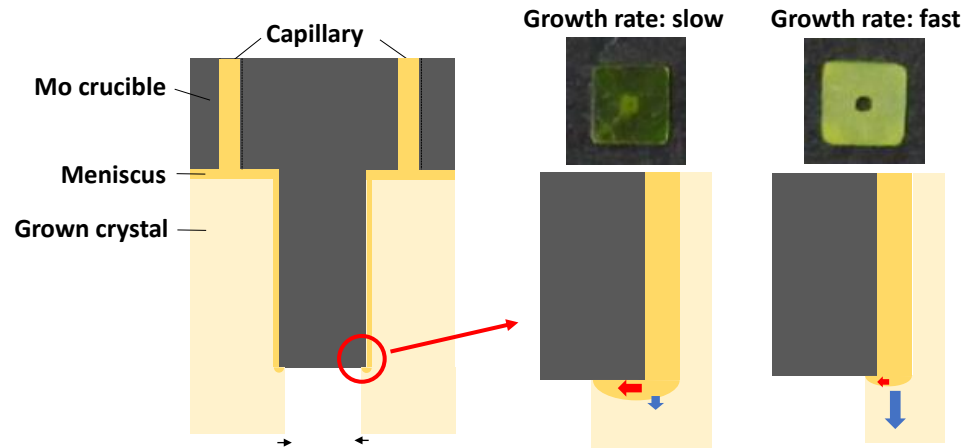


Figure 4. Schematic diagram of effect of growth speed on control of internal crystal diameter. Middle: At a slow growth rate (0.2 mm/min), the meniscus was wetted and spread at the tip of the protrusion, and the inside of the tube crystal was filled with melt. Right: At high growth rates (0.5 mm/min), the inside of the tube crystal was not filled with melt because the wetting spread of the meniscus to the tip of the protrusion was suppressed.

Ce distribution in the tangential direction of the grown crystals was measured by FE-EPMA (Figure 5). The detection limit of the FE-EPMA measurement was 210 wt. ppm. The Ce concentration around the capillary tended to be smaller than that in the remainder of the capillary area. This result agrees with our previous report on the growth of tube-YAG:Ce using Ir crucibles [17]—the small Ce concentration around capillaries was caused by the small segregation coefficient of Ce in the YAG single crystal and by small convection in the meniscus.

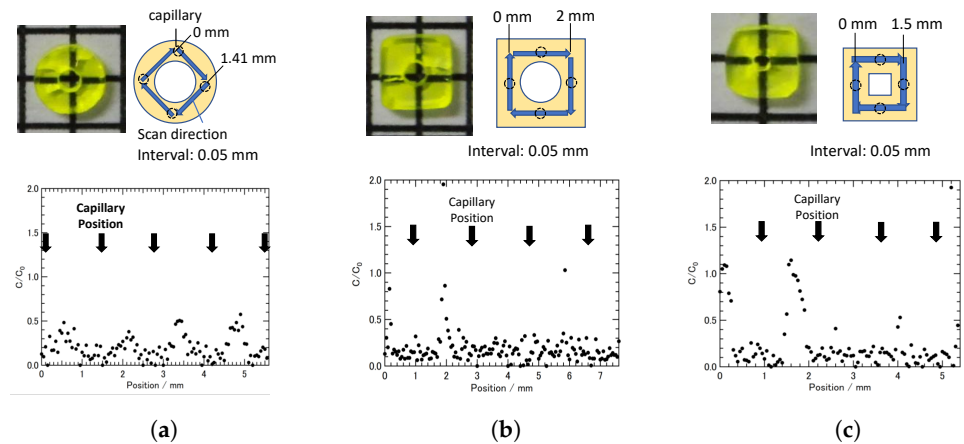


Figure 5. Ce distribution in tangential direction of grown crystals measured by FE-EPMA. (a) TYPE1 crucible. (b) TYPE2 crucible. (c) TYPE3 crucible.

3.2. Optical and Scintillation Properties

The optical transmittance spectra of the tube-YAG:Ce crystals that were grown in this study are shown in Figure 6. For all samples, two clear absorption peaks existed at 340 nm and 455 nm, which are ascribed to $4f \rightarrow 5d_2$ and $4f \rightarrow 5d_1$ absorption transitions, respectively. The transmittance above 500 nm exceeded 70% for all samples.

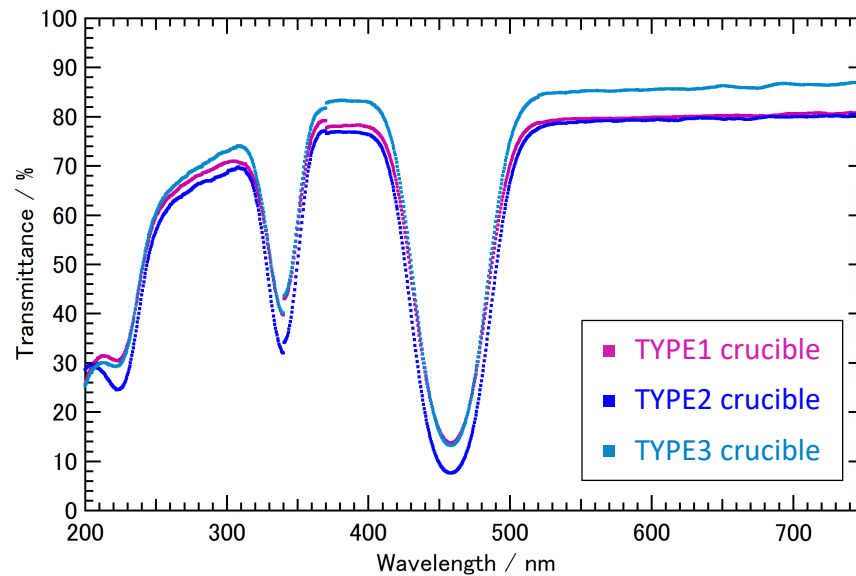


Figure 6. Optical transmittance spectra of grown crystals. In all samples, two distinct absorption bands were present at 340 nm and 455 nm, presumed to be absorption transitions at $4f \rightarrow 5d_2$ and $4f \rightarrow 5d_1$, respectively. Transmission above 500 nm was above 70% in all samples.

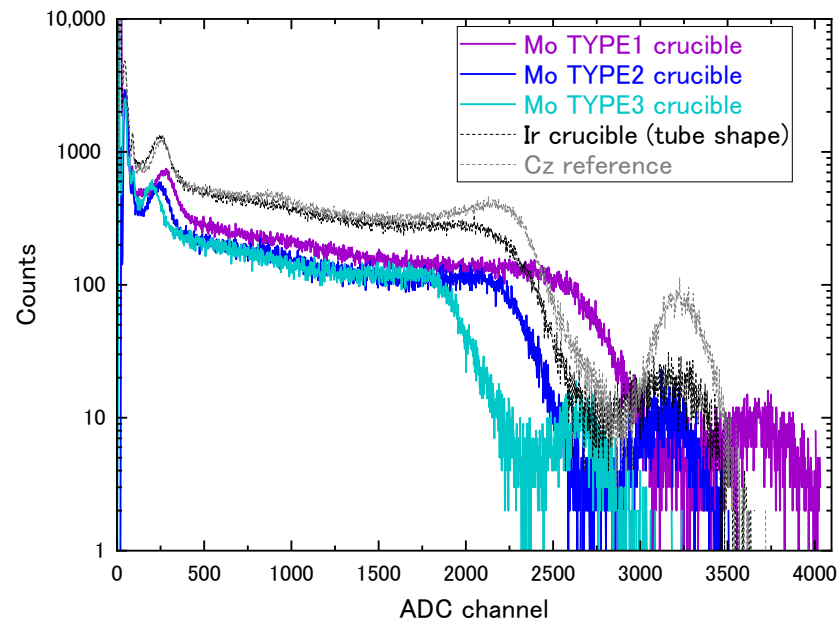
The scintillation pulse height spectra and decay curves of tube-YAG:Ce that was grown by Mo crucibles were measured (Figure 7). The pulse height spectra of Cz grown crystal and tube-YAG:Ce grown by Ir crucible are also shown in Figure 7a. The scintillation properties are summarized in Table 1. The scintillation light output (LO) of the samples were estimated by comparing the ADC channel of the ^{137}Cs 662 keV photopeak of the samples with that of the Cz sample, using the following formula:

$$LO_{\text{samples}} = LO_{\text{reference}} \times \frac{\text{Photopeak}_{\text{sample}}}{\text{Photopeak}_{\text{reference}}}$$

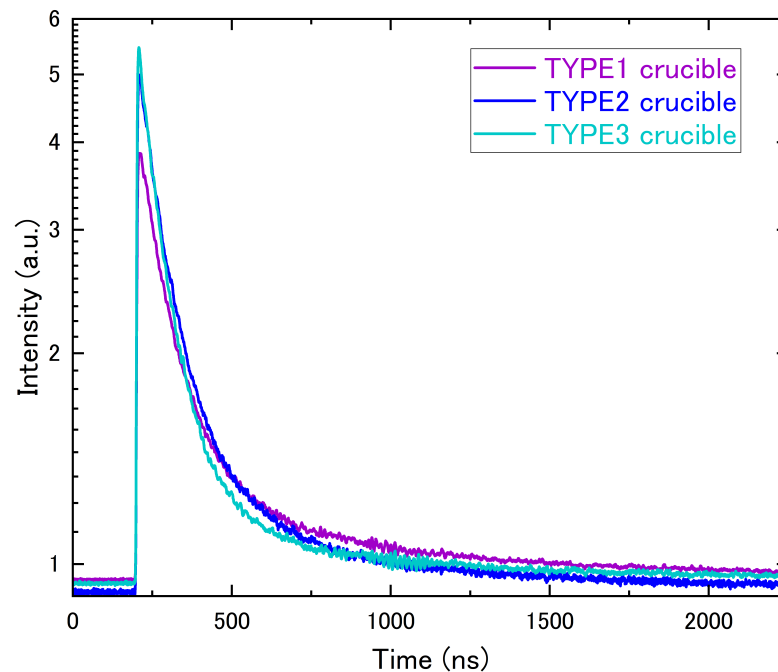
As a result, the scintillation properties of all samples were almost comparable with Cz sample.

The crystal grown in a TYPE 3 crucible was cut into 1- to 2-mm-thick pieces, and 12 samples were obtained. The scintillation light output and decay time of these samples were measured and plotted in the Figure 8 as a function of the distance from the growth start. The standard deviation (σ) of the scintillation light output (LO) of the samples was $\pm 16\%$. $LO_{1\text{mmt}}/LO_{2\text{mmt}}$ —the ratio of the average scintillation light output for the 1 mm and 2 mm thick samples—was 17%.

The radioluminescence spectra of grown tube-YAG:Ce crystals are shown in Figure 9. All sample shapes were the same with a broad-band emission and peak at 540 nm, which is typical for Ce^{3+} 5d-4f emission in YAG crystals. The small and broad emission around 250–400 nm—that is prominent in the sample grown by TYPE3 crucible—is ascribed to self-trapped exciton and YAl anti-site defects, and a possible trap candidate has been reported to be anti-site $\text{Y}_{\text{Al}}^{3+}$ defects [20]. The lower light output of the sample grown by TYPE3 crucible is most probably due to its anti-site defects.



(a)



(b)

Figure 7. Scintillation properties of YAG:Ce crystals grown by TYPE1, TYPE2, and TYPE3 crucibles. The pulse height spectra of Cz grown crystal and tube-YAG:Ce grown by Ir crucible are also shown in (a). (a) Pulse Height Spectra irradiated by ^{137}Cs source. ADC channel stands for “Analog-to-Digital Converter channel”. ADC channels represents the amplitude of the waveform. The ^{137}Cs 662 keV photopeaks were observed in all samples. (b) Average waveforms of 512 events.

Table 1. Results of scintillation property measurements.

Position	Light Output	Primary Decay	Secondary Decay
TYPE1	20,000 ph/MeV	87 ns	370 ns
TYPE2	22,000 ph/MeV	94 ns	500 ns
TYPE3	16,000 ph/MeV	79 ns	410 ns

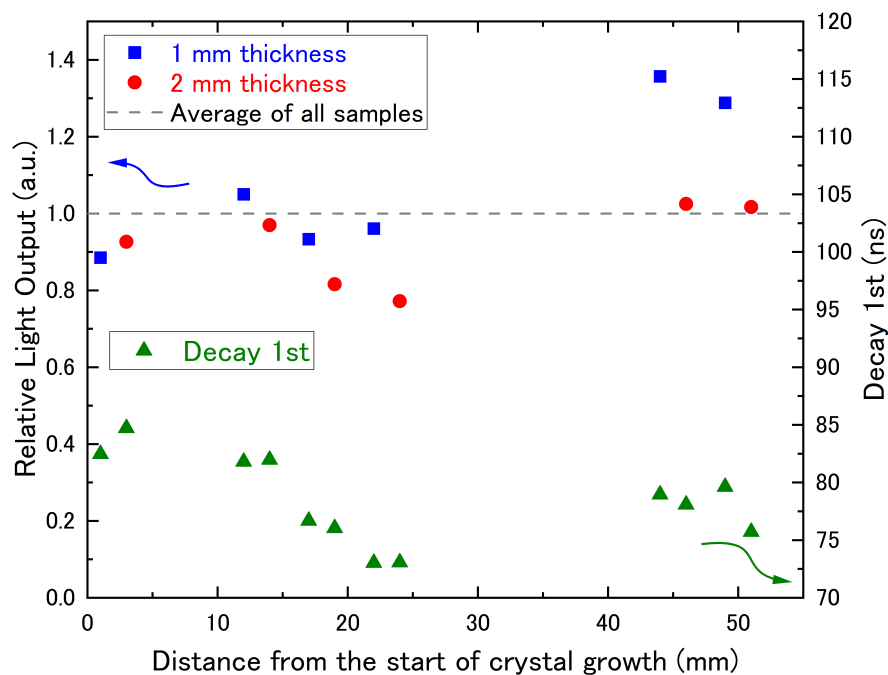


Figure 8. The scintillation properties of samples grown by TYPE3 crucible as a function of the distance from the growth start. A standard deviation (σ) of $\pm 16\%$ was achieved in scintillation light output over a 50 mm crystal length.

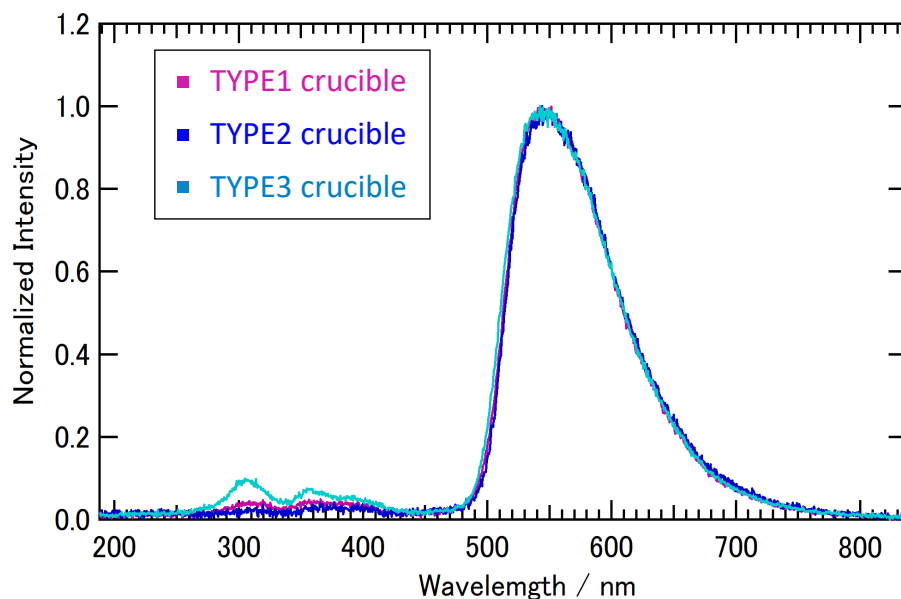


Figure 9. Radioluminescence spectra of grown crystals. All sample shapes were the same with a broad-band emission and peak at 540 nm, which is typical for Ce^{3+} 5d-4f emission in YAG crystals. The small and broad emission around 250–400 nm is ascribed to self-trapped exciton and YAl anti-site defects.

4. Conclusions

Three types of Mo crucibles with different die shapes were developed. The crucibles were applied to grow tube-YAG:Ce single crystals by using the μ -PD method. In the early stages of crystal growth, meniscus spreading into the die was unstable, and the outer diameter of the grown crystals fluctuated. After the meniscus thickness stabilized (80 μ m–100 μ m), the diameter of the grown crystals became uniform, and the cross-sectional shape of the crystals was close to that of the die. The optimum pulling-down speed for crystal-growth stabilization was faster in the crucible with a square die than that in the crucible with a round die. When grown in a crucible with a small inner diameter (TYPE 3), at a slow growth rate (0.2 mm/min), the meniscus was wetted and spread at the tip of the protrusion, and the inside of the tubular crystal was filled with melt. However, an increase in growth rate to 0.5 mm/min suppressed the filling of the interior of the tube crystal. By using TYPE3 crucible and optimizing the crystal growth rate, stable crystal growth of more than 50 mm in length was achieved with the same shape as the die. Measurements of the tangential Ce concentration distribution in the grown crystals showed that the Ce concentration around the capillary was lower than in the remainder of the crystal. The transmittance of grown crystals above 500 nm was almost the same and above 70%. The scintillation properties of the tube-YAG:Ce single crystals that were grown by Mo crucibles were comparable with those of YAG:Ce single crystals grown by the Cz method. For crystal grown by the TYPE3 crucible, the crystal was cut at thicknesses of 1 mm and 2 mm over a 50 mm range, and the variation in scintillation light output was evaluated. As a result, the standard deviation (σ) of the scintillation light output of the samples was found to be within $\pm 16\%$.

Author Contributions: Conceptualization and/or Methodology, M.Y. and Y.Y.; Resources and/or Data Curation, A.K. and T.H.; Analysis and/or Interpretation of data and/or Visualization, M.Y., A.K., Y.Y. and T.H.; Supervision, A.Y.; Writing—Original Draft Preparation, M.Y. and Y.Y.; Writing—Review and Editing, M.Y., A.K., Y.Y., T.H. and A.Y.; Approval of the version of the manuscript to be published, M.Y., A.K., Y.Y., T.H. and A.Y. All persons who meet authorship criteria are listed as authors, and all authors certify that they have participated sufficiently in the work to take public responsibility for the content, including participation in the concept, design, analysis, writing, or revision of the manuscript. Furthermore, each author certifies that this material or similar material has not been and will not be submitted to or published in any other publication before its appearance in Crystals. All authors have read and agreed to the published version of the manuscript.

Funding: This work was supported by JSPS KAKENHI [grant numbers 21H03834, 19K17191].

Institutional Review Board Statement: Not applicable.

Informed Consent Statement: Not applicable.

Data Availability Statement: Not applicable.

Acknowledgments: We would like to thank Issei Narita for his support on FE-EPMA measurement. We also thank Laura Kuhar for editing a draft of this manuscript.

Conflicts of Interest: The authors declare no conflict of interest. The funders had no role in the design of the study; in the collection, analyses, or interpretation of data; in the writing of the manuscript, or in the decision to publish the results.

References

1. Nikl, M.; Yoshikawa, A. Recent R&D Trends in Inorganic Single-Crystal Scintillator Materials for Radiation Detection. *Adv. Opt. Mater.* **2015**, *3*, 463–481. [[CrossRef](#)]
2. Shimazoe, K.; Yoshino, M.; Ohshima, Y.; Uenomachi, M.; Oogane, K.; Orita, T.; Takahashi, H.; Kamada, K.; Yoshikawa, A.; Takahashi, M. Development of simultaneous PET and Compton imaging using GAGG-SiPM based pixel detectors. *Nucl. Instruments Methods Phys. Res. Sect. A Accel. Spectrometers, Detect. Assoc. Equip.* **2020**, *954*, 161499. [[CrossRef](#)]
3. Kodama, S.; Kurosawa, S.; Ohno, M.; Morishita, Y.; Usami, H.; Hayashi, M.; Sasano, M.; Azuma, T.; Tanaka, H.; Kochurikhin, V.; et al. Fiber-read radiation monitoring system using an optical fiber and red-emitting scintillator for ultra-high-dose conditions. *Appl. Phys. Express* **2020**, *13*, 047002. [[CrossRef](#)]

4. Lee, T.; Lee, W. A cubic gamma camera with an active collimator. *Appl. Radiat. Isot.* **2014**, *90*, 102–108. [[CrossRef](#)] [[PubMed](#)]
5. Omata, A.; Kataoka, J.; Fujieda, K.; Sato, S.; Kuriyama, E.; Kato, H.; Toyoshima, A.; Teramoto, T.; Ooe, K.; Liu, Y.; et al. Performance demonstration of a hybrid Compton camera with an active pinhole for wide-band X-ray and gamma-ray imaging. *Sci. Rep.* **2020**, *10*, 14064. [[CrossRef](#)] [[PubMed](#)]
6. Kamada, K.; Yanagida, T.; Endo, T.; Tsutumi, K.; Usuki, Y.; Nikl, M.; Fujimoto, Y.; Fukabori, A.; Yoshikawa, A. 2inch diameter single crystal growth and scintillation properties of Ce:Gd₃Al₂Ga₃O₁₂. *J. Cryst. Growth* **2012**, *352*, 88–90. [[CrossRef](#)]
7. Kochurikhin, V.; Kamada, K.; Kim, K.J.; Ivanov, M.; Gushchina, L.; Shoji, Y.; Yoshino, M.; Yoshikawa, A. Czochralski growth of 4-inch diameter Ce:Gd₃Al₂Ga₃O₁₂ single crystals for scintillator applications. *J. Cryst. Growth* **2019**, *531*, 125384. [[CrossRef](#)]
8. Yoshikawa, A.; Shoji, Y.; Yokota, Y.; Kurosawa, S.; Hayasaka, S.; Chani, V.I.; Ito, T.; Kamada, K.; Ohashi, Y.; Kochurikhin, V. Growth of 2Inch Eu-doped SrI₂ single crystals for scintillator applications. *J. Cryst. Growth* **2016**, *452*, 73–80. [[CrossRef](#)]
9. Yokota, Y.; Shimoyama, J.i.; Ogata, T.; Horii, S.; Kishio, K. Dramatic effects of excess oxygen on physical properties and crystal structure of La_{0.95}Sr_{0.05}MnO_y single crystal. *Solid State Commun.* **2007**, *142*, 429–433. [[CrossRef](#)]
10. Kamada, K.; Nikl, M.; Kotaki, T.; Saito, H.; Horikoshi, F.; Miyazaki, M.; Kim, K.J.; Murakami, R.; Yoshino, M.; Yamaji, A.; et al. Multiple shaped-crystal growth of oxide scintillators using Mo crucible and die by the edge defined film fed growth method. *J. Cryst. Growth* **2020**, *535*, 125510. [[CrossRef](#)]
11. Kurlov, V.; Epelbaum, B. EFG growth of sapphire tubes upto 85mm in diameter. *J. Cryst. Growth* **1998**, *187*, 107–110. [[CrossRef](#)]
12. Yoshikawa, A.; Chani, V. Growth of Optical Crystals by the Micro-Pulling-Down Method. *MRS Bull.* **2009**, *34*, 266–270. [[CrossRef](#)]
13. Yoshikawa, A.; Satonaga, T.; Kamada, K.; Sato, H.; Nikl, M.; Solovieva, N.; Fukuda, T. Crystal growth of Ce: PrF₃ by micro-pulling-down method. *J. Cryst. Growth* **2004**, *270*, 427–432. [[CrossRef](#)]
14. Lebbou, K.; Perrodin, D.; Chani, V.I.; Brenier, A.; Tillement, O.; Aloui, O.; Fourmigue, J.M.; Didierjean, J.; Balembois, F.; Gorges, P. Fiber single-crystal growth from the melt for optical applications. *J. Am. Ceram. Soc.* **2006**, *89*, 75–80. [[CrossRef](#)]
15. Yoshikawa, A.; Nikl, M.; Boulon, G.; Fukuda, T. Challenge and study for developing of novel single crystalline optical materials using micro-pulling-down method. *Opt. Mater.* **2007**, *30*, 6–10. [[CrossRef](#)]
16. Lebbou, K. Single crystals fiber technology design. Where we are today? *Opt. Mater.* **2017**, *63*, 13–18. [[CrossRef](#)]
17. Kotaki, A.; Yoshino, M.; Yokota, Y.; Hanada, T.; Yamaji, A.; Toyoda, S.; Sato, H.; Ohashi, Y.; Kurosawa, S.; Kamada, K.; et al. Crystal growth and scintillation properties of tube shape-controlled Ce-doped Y₃Al₅O₁₂ single crystals grown by micro-pulling-down method. *Appl. Phys. Express* **2020**, *13*, 125503. [[CrossRef](#)]
18. Sidletskiy, O.; Lebbou, K.; Kofanov, D. Micro-pulling-down growth of long YAG- and LuAG-based garnet fibres: Advances and bottlenecks. *CrystEngComm* **2021**, *23*, 2633–2643. [[CrossRef](#)]
19. Tkachenko, S.; Arhipov, P.; Gerasymov, I.; Kurtsev, D.; Vasyukov, S.; Nesterkina, V.; Shiran, N.; Mateichenko, P.; Sidletskiy, O. Control of optical properties of YAG crystals by thermal annealing. *J. Cryst. Growth* **2018**, *483*, 195–199. [[CrossRef](#)]
20. Babin, V.; Blazek, K.; Krasnikov, A.; Nejezchleb, K.; Nikl, M.; Savikhina, T.; Zazubovich, S. Luminescence of undoped LuAG and YAG crystals. *Phys. Status Solidi* **2005**, *2*, 97–100. [[CrossRef](#)]